Molecular Cancer Therapeutics

The Antitumor Drug LB-100 Is a Catalytic Inhibitor of Protein Phosphatase 2A (PPP2CA) and 5 (PPP5C) Coordinating with the Active-Site Catalytic Metals in PPP5C

Brandon M. D'Arcy[1,2], Mark R. Swingle[2], Cinta M. Papke[2], Kevin A. Abney[2], Erin S. Bouska[2], Aishwarya Prakash[1,3], and Richard E. Honkanen[1,2]

Abstract

LB-100 is an experimental cancer therapeutic with cytotoxic activity against cancer cells in culture and antitumor activity in animals. The first phase I trial (NCT01837667) evaluating LB-100 recently concluded that safety and efficacy parameters are favorable for further clinical testing. Although LB-100 is widely reported as a specific inhibitor of serine/threonine phosphatase 2A (PP2AC/*PPP2CA:PPP2CB*), we could find no experimental evidence in the published literature demonstrating the specific engagement of LB-100 with PP2A *in vitro*, in cultured cells, or in animals. Rather, the premise for LB-100 targeting PP2AC is derived from studies that measure phosphate released from a phosphopeptide (K-R-pT-I-R-R) or inferred from the ability of LB-100 to mimic activity previously reported to result from the inhibition of PP2AC by other means. PP2AC and PPP5C share a common catalytic mechanism. Here, we demonstrate that the phosphopeptide used to ascribe LB-100 specificity for PP2A is also a substrate for PPP5C. Inhibition assays using purified enzymes demonstrate that LB-100 is a catalytic inhibitor of both PP2AC and PPP5C. The structure of PPP5C cocrystallized with LB-100 was solved to a resolution of 1.65Å, revealing that the 7-oxabicyclo[2.2.1]heptane-2,3-dicarbonyl moiety coordinates with the metal ions and key residues that are conserved in both PP2AC and PPP5C. Cell-based studies revealed some known actions of LB-100 are mimicked by the genetic disruption of *PPP5C*. These data demonstrate that LB-100 is a catalytic inhibitor of both PP2AC and PPP5C and suggest that the observed antitumor activity might be due to an additive effect achieved by suppressing both PP2A and PPP5C.

Introduction

The reversible phosphorylation of proteins regulates many aspects of cell growth and metabolic homeostasis. Therefore, compounds that specifically manipulate key phosphorylation-regulated processes should be useful in the medical management of human disease. Indeed, over 25 FDA-approved drugs used to manage human cancers target protein kinases (1, 2). In contrast, the development of drugs targeting protein phosphatases received little attention until recently, when it became clear that, like their kinase counterparts, protein phosphatases are responsive and highly regulated enzymes (3).

To date, the only FDA-approved drugs targeting ser/thr phosphatases are cyclosporine, the macrolide tacrolimus (FK506), and related compounds, which are immunosuppressive agents that specifically inhibit PP2B/calcineurin (encoded by *PPP3C*; ref. 4). However, several natural compounds that target PPP-family phosphatases (i.e., fostriecin, cytostatin A, cantharidin, and tautomycetin) have impressive antitumor activity in cell culture and animal models (5–11). Fostriecin and cytostatin A are structurally related natural compounds produced by *Streptomyces* (12). Fostriecin entered clinical development due to its potent and efficacious antitumor activity nearly a decade before it was shown to act as a potent catalytic inhibitor of PP2AC (13). More rigorous analysis later revealed that fostriecin also acts as a potent inhibitor of PPP4C and as a weaker inhibitor of PPP1C and PPP5C (6, 11, 14). In the largest phase I trial conducted with fostriecin, disease stability was observed in 16 (of 46) solid tumor patients without reaching dose-limiting toxicity (15). Unfortunately, the study was closed before establishing the maximum tolerated dose (MTD) due to problems with the supply of fostriecin (15).

Cantharidin, a natural compound made by many species of blister beetles, is the active constituent in traditional Chinese medicine used for more than two millennia for a variety of purposes (5). Cantharidin was used briefly as an internal medicine in Europe, and in China, it was reported to have anticancer activity in patients with gastrointestinal cancer when used as a beetle extract (*Mylabris*; ref. 16). Cantharidin was also first reported to act as an inhibitor of PP2A in 1992 (17). Again, more rigorous testing revealed that cantharidin acts as a catalytic

[1]USA Mitchell Cancer Institute, Mobile, Alabama. [2]Department of Biochemistry and Molecular Biology, University of South Alabama, Mobile, Alabama. [3]Department of Pharmacology, University of South Alabama, Mobile, Alabama.

Note: Supplementary data for this article are available at Molecular Cancer Therapeutics Online (http://mct.aacrjournals.org/).

B.M. D'Arcy and M.R. Swingle contributed equally to this article.

Corresponding Authors: Richard E. Honkanen, University of South Alabama College of Medicine, 307 University Boulevard N, MSB 2362, Mobile, AL 36609. Phone: 251-460-6859; Fax: 251-460-6850; E-mail: rhonkanen@southalabama.edu; and Aishwarya Prakash, USA Mitchell Cancer Institute, University of South Alabama, Mobile, AL 36604. E-mail: aprakash@health.southalabama.edu

doi: 10.1158/1535-7163.MCT-17-1143

inhibitor of ser/thr phosphatases 1, 2A, 5, and 6 (PPP1C/*PPP1C*, PPP2AC/*PPP2CA/B*, PPP5C/*PPP5C*, PPP6C/*PPP6C*) with submicromolar to low micromolar affinity (5, 9). In nonprescription formulations, cantharidin is currently used to treat a variety of skin lesions. However, cantharidin is considered by many as too toxic for mainstream oncology (5), and modern clinical trials have not been attempted. Microcystin (18) and nodularin (19) are highly potent ($IC_{50} < 2$ nmol/L) but nonselective inhibitors of the cantharidin-sensitive phosphatases (i.e., PPP1C/PPP2AC/PPP5C/PPP6C). Both demonstrate marked systemic toxicity, notably hepato- and nephro-toxicity, arguing that potent nonselective inhibitors cannot be developed into useful medications.

It is assumed that the development of highly selective inhibitors of PPP-family phosphatases will generate compounds that have less systemic toxicity, and it is hoped that some selective inhibitors will retain antitumor activity. The simple structure (Fig. 1) and ease of chemical synthesis make the cantharidin/endothall scaffold attractive for the development of specific inhibitors (9, 20). Indeed, derivatives that do not inhibit PP4C have already been developed (9). LB-100 (3-(4-methylpiperazine-1-carbonyl)-7-oxabicyclo[2.2.1]heptane-2-carboxylic acid) represents the first endothall-based derivative to enter human clinical trials (21, 22). LB-100 is membrane permeable and was well tolerated in animal studies. Preclinical studies revealed that when used to supplement existing antitumor agents (e.g., cisplatin, doxorubicin, temozolomide, focal X-rays) against pancreatic (23), nasopharyngeal (24), hepatocellular carcinoma (25), fibrosarcoma (26), and glioblastoma xenografts (22), LB-100 increased potency without limiting toxicity (21, 23, 27). Recently, the first phase I clinical trial had a favorable outcome (21), and a second trial is in progress.

PPP5C (commonly called PP5 or PP5C) shares a common catalytic mechanism with PP2AC, and the ten amino acids that coordinate the catalytic metals as well as position and orient the substrate phosphoryl moiety for nucleophilic attack at the catalytic site are identical in both enzymes (28). Because inactivating alterations of PP2A subunits have been observed in human cancers and the suppression of the same PP2A components contribute to cell transformation (for review, see ref, 29), many view PP2A as a tumor suppressor. In contrast, PPP5C is found in high levels in several types of human cancers (30–35), and many lines of evidence indicate that inhibitors of PPP5C may prove useful for the medical management of several types of human cancers (30, 32, 36–43). Therefore, when several carboxamide derivatives containing the 7-oxabicyclo[2.2.1]heptane-2-carboxylic acid moiety shared with LB-100 were identified as novel inhibitors of PPP5C in an ultra-high-throughput screening campaign (44), we were prompted to test LB-100 for inhibitory activity against PPP5C. The data reported here represent the most comprehensive assessment of LB-100 activity against PP2AC reported to date, confirming the inhibitory activity of LB-100 against PP2AC. In addition, our studies identify PPP5C as a second LB-100–sensitive phosphatase. Structural studies using X-ray crystallography revealed that the 7-oxabicyclo[2.2.1]-heptane-2,3-dicarbonyl moiety of LB-100 is positioned over the catalytic metals of PPP5C, blocking substrate access.

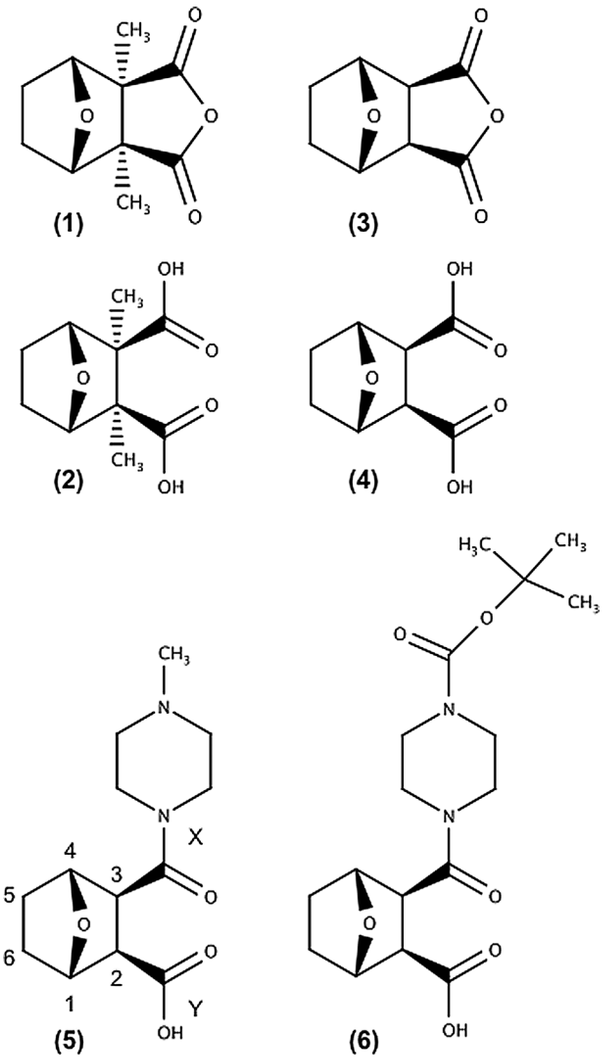

Figure 1.
Cantharidin family of inhibitors and structural derivatives. Structures of (1) cantharidin, (2) cantharidic acid, (3) norcantharidin, (4) norcantharidic acid (endothall), (5) LB-100, and (6) LB-102. All members of the cantharidin-like family of inhibitors share a common 7-oxabicyclo[2.2.1]heptane-2,3-dicabonyl moiety.

Materials and Methods

Materials

LB-100 (3-(4-methylpiperazine-1-carbonyl)-7-oxabicyclo[2.2.1]heptane-2-carboxylic acid) was purchased from MedChem Express (HY-18597). Additional materials are provided in Supplementary Material.

Cell culture

U-937 monocytes were obtained from the ATCC (CRL-1593.2) and cultured in RPMI-1640 media (Gibco, Life Technologies) supplemented with 1x nonessential amino acids, 100 units/mL penicillin, 100 μg streptomycin, and 10% FBS (Atlanta Biologicals). HEK-293 cells (ATCC CRL-1573) were cultured in DMEM supplemented with 1x L-glutamine, pyruvate, nonessential amino acids, 100 units/mL penicillin, 100 μg streptomycin (Gibco), and 10% FBS. Mycoplasma testing was performed using PCR (eMYCO Plus kit, iNtRON Biotechnology). Upon receipt from the ATCC, cell lines are routinely expanded and frozen. Following thawing, cell lines are generally discarded after 10 to 15 passages. Because the

passage log for the U-937 cells in this study was not complete, the U-937 cell line was authenticated by Genetica Cell Line Testing using short tandem repeat DNA profiling and confirmed as authentic using both the percent identity algorithm and percent match algorithm (ANSI/ATCC ASN-0002-2011). All cells were grown at 37°C with 5% CO_2 in a humidified incubator. The PPP5C-KO cells will be provided for research purposes upon request.

Western analysis

HEK-293 wild-type or HEK-293 PPP5C-KO cells (2×10^5) were plated in 60 mm dishes and allowed to grow until the culture reached a confluent monolayer. The cells were then treated with the indicated concentration of LB-100 dissolved in H_2O. After 3 hours, the cells were washed with PBS and lysed by scraping in near-boiling 2x SDS-PAGE sample buffer (62.5 mmol/L Tris-HCl, pH 6.8, 20% glycerol, 4% SDS, 0.0025% bromophenol blue, and 0.02% ß-mercaptoethanol). Cell debris was sedimented by centrifugation at 16,900 × *g* for 15 minutes. The supernatant was transferred to a new tube, protein concentrations were estimated using RC DC Protein Assay (Bio-Rad #5000121), and 50 µg of each protein sample was separated by SDS-PAGE (10% polyacrylamide gels). Proteins were then transferred onto an Immobilon-P Membrane (Millipore). The membranes were blocked at room temperature for 1 hour in Odyssey blocking buffer (LiCor) and then incubated overnight with 1:2,000 dilution of primary antibodies P-S6 (S235/236; Cell Signaling Technology #2211) or ß-actin (Sigma #A2228) in 5% BSA at 4°C. The next day, membranes were incubated with either anti-mouse (Sigma #A5278) or anti-rabbit (GE healthcare #NA934V) secondary horseradish peroxidase–conjugated antibodies (diluted at 1: 10,000) for 1 hour at room temperature. Bands were visualized using Clarity Western ECL Substrate (Bio-Rad #170-5060) using a Fuji-LAS-100 imaging system. Image J software was used for quantification of band density.

Cell viability assays

U-937 cell viability was assessed using a resazurin-based fluorescence assay (45). For IC_{50} determination, U-937 cells were seeded (1.5×10^4 cells/well) in costar black 96-well clear-bottom plates with LB-100 serially diluted with or without 500 nmol/L dexamethasone to generate the indicated final concentrations. Following 48 hours, the resazurin solution (for details, see Supplementary Material) was added to reach a final concentration of 120 µmol/L and incubated for 24 hours. At 72 hours, the relative fluorescence was measured at 540 ± 20 nm excitation and 620 ± 20 nm emission on a Tecan Infinite M1000 Pro multimode plate reader. All assays were conducted in quadruplicate, and the mean ± SD was derived from the cumulative data generated from four separate experiments ($n = 16$).

Phosphatases, substrates, and phosphatase assays

Human PPP5C was purified as previously described (6, 46, 47). Briefly, recombinant human PPP5C was expressed in *Escherichia coli* as a maltose-binding protein (MBP) fusion and purified by immobilized metal affinity chromatography. Following protease treatment, PPP5C was separated from MBP and other contaminants by anion exchange chromatography using previously described methods (46). The amino acid sequences of human and bovine PP2AC share 100% identity, making bovine PP2AC a surrogate for the human PP2AC. PP2AC was purified from bovine blood using ammonium sulfate fractionation, affinity (HiTrap heparin), and ion-exchange (HiTrap Q) chromatography according to established procedures (6). Details for all methods are provided as Supplementary Material.

[^{32}P]-phosphohistone was prepared by the phosphorylation of bovine brain histone with cAMP-dependent protein kinase (PKA) in the presence of cAMP and [^{32}P]-ATP using established methods (46, 47). DiFMUP (6,8-Difluoro-4-methylumbelliferyl phosphate; from Invitrogen)-based inhibition assays were conducted as described (46, 47) in a 96-well format using 100 µmol/L DiFMUP (final assay concentration). Phosphopeptide (KRpTIRR)/malachite green–based inhibition assays were conducted using the EMD Millipore PP2A Phosphatase Assay Kit (catalog number 17-313) using the methods, buffers, and reagents provided. In some assays, PP2AC was replaced with PPP5C as indicated. Phosphohistone phosphatase assays were performed as described (46, 47). Briefly, LB-100, at indicated concentrations, or vehicle control (H_2O) were added to enzyme/buffer aliquots approximately 10 minutes prior to starting assays by the addition of [^{32}P]-phosphohistone substrate (to a final assay concentration of 300 nmol/L incorporated phosphate). Phosphatase activity was measured by the quantification of [^{32}P]-labeled orthophosphate liberated from the substrate using established protocols (47).

Crystallization and data collection

PPP5C was combined in a 1:2.5 molar ratio with LB-100. Crystals of the PPP5C-LB-100 complex were obtained using sitting-drop vapor diffusion experiments at 16°C using 10 mmol/L Tris-HCl, pH 8.0, 35% MPD, and 10% PEG-MME 5000 as the crystallization reagent combined in a 1:1 ratio with the concentrated protein-inhibitor complex. Crystals were obtained after approximately 3 days and grew to approximately 100 × 50 µm. The crystals were mounted onto MiTeGen micro loops and flash cooled by plunging into liquid nitrogen. The data were collected in-house using an IµS 3.0 microfocus source (INCOATEC) and PHOTON II CPAD detector (Bruker). Data (60 seconds per exposure) were collected to 1.65 Å with a crystal-to-detector distance of 70 mm and an image width of 0.5° per frame. Data were processed and reduced using the PROTEUM III program suite (Bruker, AXS). Data collection statistics are summarized in Table 2.

Structure determination and refinement

Orthorhombic crystals of the PPP5C-LB-100 protein complex belonging to the $P2_12_12_1$ space group contained 1 molecule per asymmetric unit. The structure of the PPP5C-LB-100 complex was solved using molecular replacement with Phaser-MR (48) using the crystal structure of PPP5C (PDB: 1S95) as a starting model (28). Water molecules were updated during refinement and manually checked. Refinement was performed using Phenix. Refine (49). Model building and map fitting were performed in COOT (50, 51). The final model for the structure was found to exhibit good geometry, as determined using MolProbity (PHENIX; ref. 52). Refinement statistics are shown in Table 2. All structure figures were prepared using PyMOL (The PyMOL Molecular Graphics System, Version 1.8 Schrödinger, LLC).

Protein data bank accession code

Atomic coordinates and structure factor amplitudes have been deposited with the Protein data bank (http://www.pdb.org) and are accessible under accession code 5WG8.

Results

Inhibition of phosphatase activity by LB-100

Although LB-100 is widely reported to act as a specific inhibitor of PP2AC (22), we could not find a report testing the inhibitory activity of LB-100 against PPP5C, which has an identical catalytic mechanism (28) and shares several common substrates with PP2AC (53–55). Further scrutiny of the literature revealed that the ability of LB-100 to inhibit the catalytic activity of PP2A is based on studies using a commercial assay (Millipore ser/thr phosphatase assay kit). In this kit, PP2A activity is measured using a small phosphopeptide (K-R-pT-I-R-R) substrate (22, 23). When we tested the ability of PPP5C to also utilize the peptide substrate provided in the PP2A-assay kit, we observed that K-R-pT-I-R-R is also an excellent substrate for PPP5C (10,670 ± 90 nmol/L/min/mg). We next tested the ability of LB-100 to inhibit PP2AC and PPP5C in head-to-head assays using the malachite green–based assay provided in the Millipore Kit, substituting PPP5C for PP2AC as indicated. These studies revealed that LB-100 inhibits the catalytic activity of both PP2AC and PPP5C in a dose-dependent manner (Fig. 2A; Table 1).

Because LB-100 is a low-molecular-weight inhibitor (MW = 268.31), it is predicted to disrupt limited but key substrate-enzyme contacts. Therefore, we next tested the inhibitory activity of LB-100 using DiFMUP, a low-molecular-weight (MW = 292.13) fluorogenic substrate expected to interact with phosphatase active sites primarily via limited contacts with its phosphoryl moiety. As observed with the malachite green–based assay, when DiFMUP is used as a substrate, LB-100 inhibits the activity of both PP2AC and PPP5C (Fig. 2B).

Although LB-100 was found to be a potent inhibitor of both PP2AC and PPP5C with small nonphysiologic substrates, interaction between protein phosphatases and their substrates can occur over relatively large domains that produce multiple contacts. Therefore, we next tested the ability of LB-100 to inhibit the activity of PP2AC and PPP5C using protein kinase A phosphorylated [^{32}P]-histone, which is an established substrate for both PP2AC and PPP5C (6, 28, 44, 46, 47). As observed using DiFMUP or K-R-pT-I-R-R as a substrate, the dephosphorylation of [^{32}P]-radiolabeled phosphohistone by PP2AC is potently inhibited by LB-100. When tested against PPP5C, we found that LB-100 again also inhibits PPP5C activity in a concentration-dependent manner (Fig. 2C; Table 1). With all three substrates, LB-100 demonstrated modest (~4–7-fold) selectivity for PP2AC versus PPP5C. Together, these studies confirm that LB-100 is a catalytic inhibitor of PP2AC and identified PPP5C as a second LB-100–sensitive phosphatase.

Table 1. Inhibitory activity of LB-100 against PP2AC and PPP5C[a]

	Phosphatase; IC_{50} mean ± SE (μmol/L)[b]	
Substrate	**PP2AC**	**PPP5C**
DiFMUP	0.39 ± 0.013	1.82 ± 0.093
[^{32}P]-Labeled phosphohistone	0.64 ± 0.037	4.9 ± 0.29
(K-R-pT-I-R-R)	1.27 ± 0.13	6.64 ± 0.24

[a]Phosphatase activity was measured as described in Materials and Methods.
[b]IC_{50} values are calculated from a 9-, 10-, or 11-point concentration/dose-response curve by a 4-parameter logistic fit of the data, using 3 to 8 replicates per concentration.

Table 2. Data collection, phasing, and refinement statistics for PP5C cocrystallized with LB-100

PDB code	**5WG8**
Beamline	Home source (D8 Quest, Bruker)
Wavelength (Å)	1.5418
Space group	$P2_12_12_1$
Unit-cell parameters (Å, °)	$a = 40.656$, $b = 91.15$, $c = 95.494$ $\alpha = \beta = \gamma = 90$
Molecules per asymmetric unit	1
Data collection statistics	
Resolution range (Å)	30.34–1.65 (1.709–1.65)
Unique reflections	43,438 (4,165)
Redundancy	8 (3.6)
R_{merge}	0.142 (0.738)
R_{meas}	0.151 (0.854)
R_{pim}	0.050 (0.420)
$CC_{1/2}$	0.990 (0.671)
Overall I/σ	23.6 (3.5)
Completeness (%)	99.7 (97.5)
MR phasing statistics	
Top LLG	3125.995
Top TFZ	44.4
Refinement statistics	
Reflections used in refinement	43,429 (4,160)
Reflections used for R_{free}	4,300 (436)
R_{work} (%)	0.1587 (0.3047)
R_{free} (%)	0.1961 (0.3472)
Number of nonhydrogen atoms	2,890
Macromolecules	2,599
Ligands	29
Solvent	262
r.m.s.d values	
Bond length (Å)	0.009
Bond angles (°)	0.96
B-factor (Å^2)	
Wilson B	9.72
Protein	8.68
Ligand	15.04
Water	19.47
Ramachandran plot	
Ramachandran favored (%)	96.54
Ramachandran allowed (%)	3.46
Ramachandran outliers (%)	0
Clashscore	1.93

NOTE: $R_{merge} = \Sigma|I-\langle I\rangle|/\Sigma I$, where $\langle I\rangle$ is the average intensity from multiple observations of symmetry-related reflections; R_{work} and $R_{free} = \Sigma||F_o| - |F_c||/\Sigma|F_o|$, where F_o and F_c are the observed and calculated structure factor amplitudes, respectively. R_{free} was calculated with 10% of the reflections not used in refinement. Values for the highest resolution shell are shown in parentheses.
Abbreviation: MR, molecular replacement.

Sensitivity of the U-937 cells to LB-100

Thorough review of the literature revealed that the premise that LB-100 targets PP2A in cells or tissues is derived from studies in which cells or animals were treated with LB-100 and the lysates from untreated and treated cells/tissues were compared (22, 56–64). This was done by measuring either: (1) the ability of the LB-100–treated lysates to inhibit the activity of PP2A when only PP2AC was added to the assay; (2) measuring the release of phosphate from a phosphopeptide (K-R-pT-I-R-R) added to the lysates under the assumption that this represents PP2AC activity; or (3) by assessing LB-100–induced changes in the phosphorylation of proteins that were previously reported to occur when PP2A was inhibited by other means [i.e., studies with okadaic acid, which inhibits both PP2A and PPP5C, or with siRNA/antisense oligonucleotides that specifically suppress the

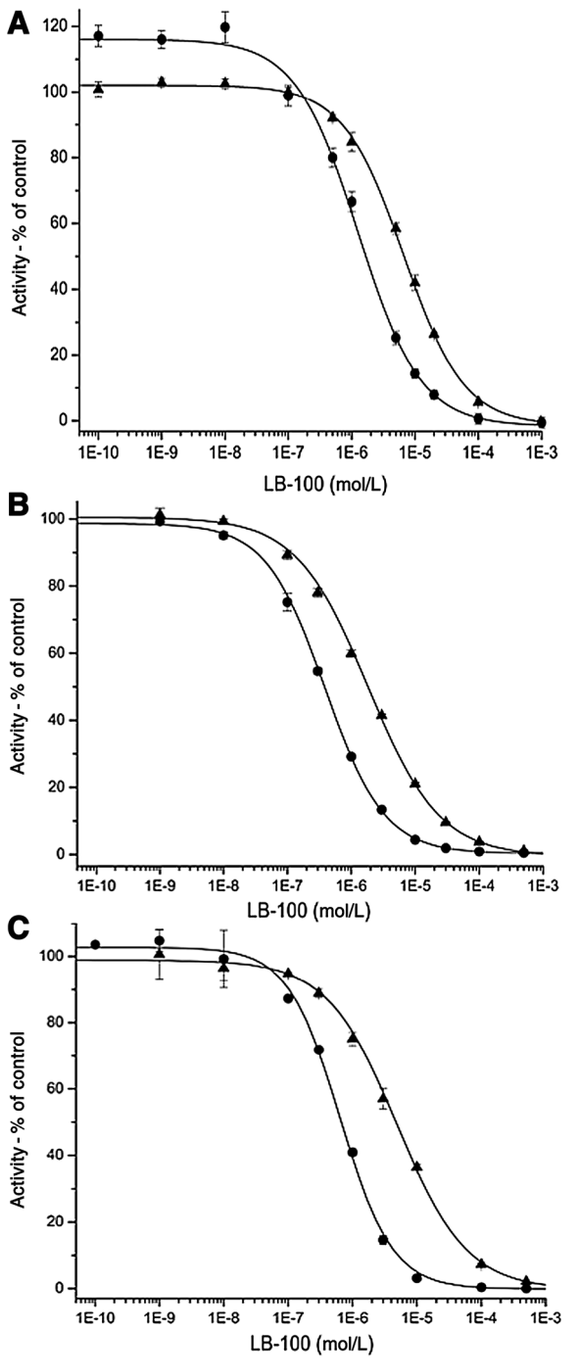

Figure 2.

Inhibitory effect of LB-100 on the activity of PP2AC and PPP5C. Inhibition of PP2AC (circles) and PPP5C (triangles) activity by LB-100 assayed using (**A**) a phosphopeptide (K-R-pT-I-R-R), (**B**) DiFMUP, or (**C**) [^{32}P]-labeled histone as a substrate. Assays were conducted as described in Materials and Methods. All compounds were mixed with the enzymes for $\geq$10 minutes at 23°C prior to the initiation of the reaction with the addition of substrate. Each point represents the mean $\pm$ SD ($n = 3$–8). IC_{50} values calculated from a 9-, 10-, or 11-point concentration/dose-response curve by a 4-parameter logistic fit of the data are provided in Table 1.

expression of PP2AC or PPP2R1A (a regulatory/scaffold protein needed to properly assemble the PP2A holoenzyme; ref. 65)].

Having demonstrated that the phosphopeptide used to measure PP2A activity is readily dephosphorylated by both PP2AC and PPP5C (Fig. 2A) and that LB-100 inhibits both PP2AC and PPP5C at similar concentrations *in vitro* (Fig. 2), we next conducted cell-based studies to determine if LB-100 can elicit actions altered by the inhibition of PPP5C but not by the inhibition of PP2A. Although PP2A and PPP5C act on several common substrates, the ability of arachidonic acid (AA) to activate PPP5C but not PP2A has been established for nearly two decades (66, 67). In response to oxidative stress, the activation of PPP5C leads to the suppression of both ASK1-induced apoptosis (68–71) and dexamethasone-induced glucocorticoid receptor (GR) action (72–74). In cells belonging to the monocyte/macrophage lineage (e.g., U-937 cells), production of AA provides a survival advantage during periods of oxidative stress that can be suppressed by dexamethasone (Fig. 3A; refs. 75–77). Therefore, if LB-100 acts to suppress the actions of PPP5C, the cytotoxic activity of LB-100 should be augmented by treatment with dexamethasone. To test this, we conducted dose-response studies in the presence or absence of 500 nmol/L dexamethasone using a metabolic capacity assay (resazurin-based fluorescence) as a surrogate to assess toxicity (Fig. 3B). These studies revealed that the cytotoxic activity of LB-100 is indeed modestly increased in the presence of 500 nmol/L dexamethasone (Fig. 3B), consistent with the notion that LB-100 is inhibiting PPP5C in U-937 cells.

Because most compounds used to inhibit PP2A activity in cells or animals (i.e., okadaic acid, calyculin A, cantharidin, endothall, microcystin, nodularin, tautomycetin) also inhibit PPP5C at similar concentrations (78), we used a CRISPR-Cas9–based approach to generate stable clonally derived HEK-293 cell lines in which the expression of PPP5C was disrupted by inserting a single base leading to a frameshift-induced stop codon in exon one (79). In the PPP5C-deficient HEK-293 cells, we found that phosphorylation of ribosomal S6 (Ser235/236) is constitutively elevated. To determine whether LB-100 targeted the activity of PPP5C in a cellular context, we conducted dose-response studies by treating wild-type cells with LB-100 and assessed S6 (Ser235/236) phosphorylation status. We found that phosphorylation of ribosomal protein S6 (Ser235/236) was induced in the wild-type HEK-293 cells by LB-100 in a dose-dependent manner (Fig. 3C), again mimicking the activity achieved by the specific suppression of PPP5C (Fig. 3D).

Crystal structure of PPP5C in complex with LB-100

To further understand the inhibitory activity of LB-100 against PPP5C, the structure of PPP5C cocrystallized with LB-100 was solved to a resolution of 1.65 Å (Table 2). The active site of PPP5C (identified by two closely apposed metal ions) is located at the base of a shallow depression on the surface formed by residues from four loops connecting secondary structural elements in the protein: β4-αD, αG-αH, β10-β11, and β12-β13 (28). The structure reveals clear density for the 7-oxabicyclo[2.2.1]heptane-2,3-dicarbonyl moiety (Fig. 4A). However, there was insufficient density to position the 3-[4-methyl-1-piperazine] ring. Thus, we modeled the minimal 7-oxabicyclo[2.2.1]heptane-2,3-dicarbonyl moiety of LB-100 into the observed density. To corroborate this observation, we also examined our data using isomorphous difference methods with the PP5C-4TE complex (PDB ID: 4ZX2). The difference map obtained indicated that the C5 methyl group

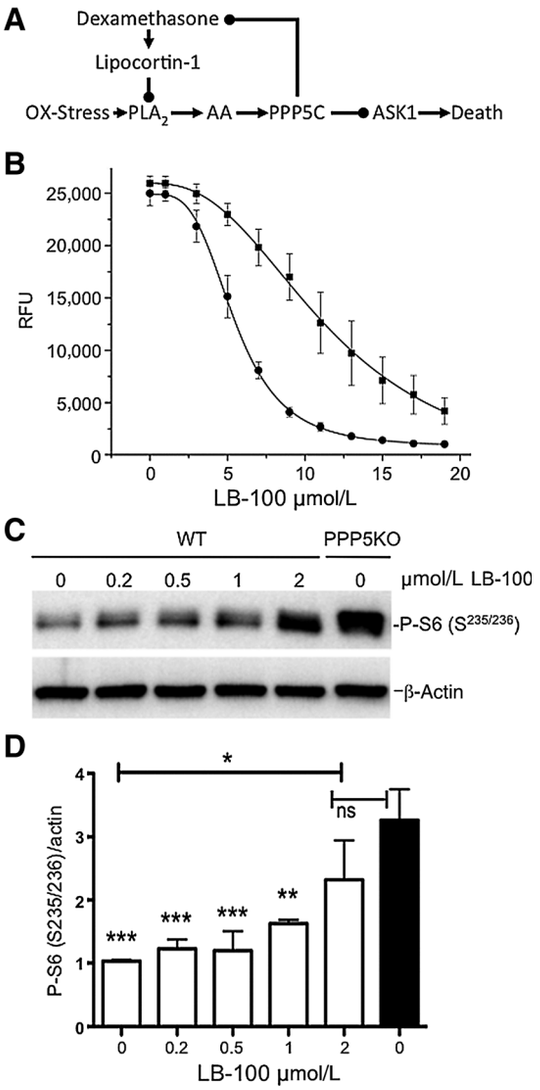

Figure 3.

The impact of LB-100 treatment on PPP5C in human cells. **A,** Schematic of known cytoprotective roles for PPP5C. Dexamethasone-stimulated expression of lipocortin-1 suppresses oxidative stress–induced release of AA by phospholipase A_2 (PLA_2). PPP5C is activated by AA, and activated PPP5C suppresses apoptosis signaling kinase 1 (ASK1)–mediated cytotoxicity. **B,** The cytotoxicity of LB-100 in U-937 cells is augmented by the addition of dexamethasone. Representative dose-response curves plotted as the relative fluorescent units (RFU) generated using the resazurin-based fluorescent assay versus the final concentration of LB-100. Square: LB-100 alone, $EC_{50} = 11.7 \pm 0.49$ μmol/L; circle: LB-100 and 500 nmol/L dexamethasone, $EC_{50} = 5.48 \pm 0.073$ μmol/L. Fluorescent measurements were made 72 hours after LB-100 was added to the cultures. All assays were conducted in quadruplicate, and the mean ± SD shown was derived from the cumulative data generated from four separate experiments ($n = 16$). **C,** Representative Western blot comparing S6 phosphorylation in cell extracts generated from wild-type (WT) HEK-293 cells treated with the indicated concentration of LB-100, and untreated HEK-293 cells in which the expression of PPP5C was disrupted (PPP5KO) using CRISPR-Cas9–based methods. HEK-293 cells were treated with the indicated concentration of LB-100 (0–2 μmol/L) for 3 hours, and phosphorylation of ribosomal S6 at S235 and S236 was detected using a phospho-specific antibody as described in Materials and Methods. **D,** Quantitation of Western blot normalized to β-actin; ns, not significant; *, $P < 0.05$; **, $P < 0.01$; and ***, $P < 0.001$.

in 4TE was not present, and no apparent density was revealed for the methylpiperazine ring of LB-100 (Supplementary Fig. S1). Because there was ambiguity associated with placing the 3-[4-methyl-1-piperazine] ring in our model, the ring and apposing oxygen atoms of the 2,3-carbonyl were not included and assigned as positions X and Y for demonstrative purposes (Fig. 4).

Our structure superposes well with other PPP5C structures (r.m.s.d. values reported in Supplementary Table S1). From the superposition of our current model with the PPP5C-phosphate complex (PDB ID: 1S95), it is apparent that the two Mn^{2+} ions (M1, M2) occupy the same positions (Fig. 4C). However, the coordination geometry between the active-site residues and the metal ions differs from 1S95 due to the presence of the inhibitor (Fig. 4B and C). In the PPP5C-phosphate complex, both active-site metals exhibit a slightly distorted octahedral geometry, interacting with six PPP5C active-site residues and two coordinated waters (one being the attacking nucleophile in the phosphomonoester hydrolysis reaction; ref. 28). With LB-100 bound, M2 maintains an octahedral sphere where coordination is mediated by PPP5C residues Asp242, His244, and Asp271 as well as three oxygen atoms of the inhibitor (the O7 bridging oxygen, and the 2,3-carbonyl groups; Fig. 4B). On the other hand, M1 displays trigonal bipyramidal coordination geometry, interacting with four PPP5C residues (Asp271, Asn303, His352, and His427) and the 2-carbonyl of LB-100. When comparing the PPP5C-phosphate substrate analog complex to the PPP5C–LB-100 complex, we observe that the bridging water/hydroxide is replaced by the 2-carbonyl of LB-100, which coordinates both M1 and M2. The water coordinating with M2 is replaced by the O7 bridging oxygen, whereas the phosphate oxygen in 1S95 coordinating M2 is substituted by the 3-carbonyl group of LB-100 (Fig. 4C). Thus, in the PPP5C-LB-100 complex, the inhibitor occupies the coordination sites for the substrate phosphoryl moiety and the two active-site waters. In addition, in order to accommodate the inhibitor, the side chains of Arg275 and Tyr451 adopt conformations slightly farther away (2.0 Å for CZ of Arg275 and 1.6 Å for the hydroxyl of Tyr451) from the active-site metals (Fig. 4B).

The substrate-binding pocket harbors several conserved active-site residues (i.e., Arg275, His304, Arg400, and His427) that participate in a complex network of hydrogen bonding interactions. Arg275 and His304 are stabilized by H-bonds with Tyr451 and Asp274, respectively, whereas Arg400 donates a hydrogen bond to the carbonyl oxygen of His427. Further stabilization of the complex is provided by hydrophobic contacts between the inhibitor and the side chains of Val429, Phe446, and Tyr451 as well as an antiparallel dipole–dipole stacking interaction between the 3-carbonyl of LB-100 and the backbone carbonyl of His427 [(C···O) = 3 Å and 3.3 Å; Fig. 4B].

Discussion

In preclinical studies, LB-100 was shown to inhibit proliferation and induce apoptosis in a variety of cultured cancer cells. LB-100 also acts as an effective chemo- and radiosensitizer for the treatment of various cancers, and LB-100 exhibited potent *in vivo* antineoplastic activity in combination with cisplatin or doxorubicin in mouse xenograft models (21, 23, 25, 27, 80, 81). The first-in-human phase I trial (NCT01837667) recently concluded that the safety, tolerability, and preliminary evidence of antitumor activity support the continued development of LB-100

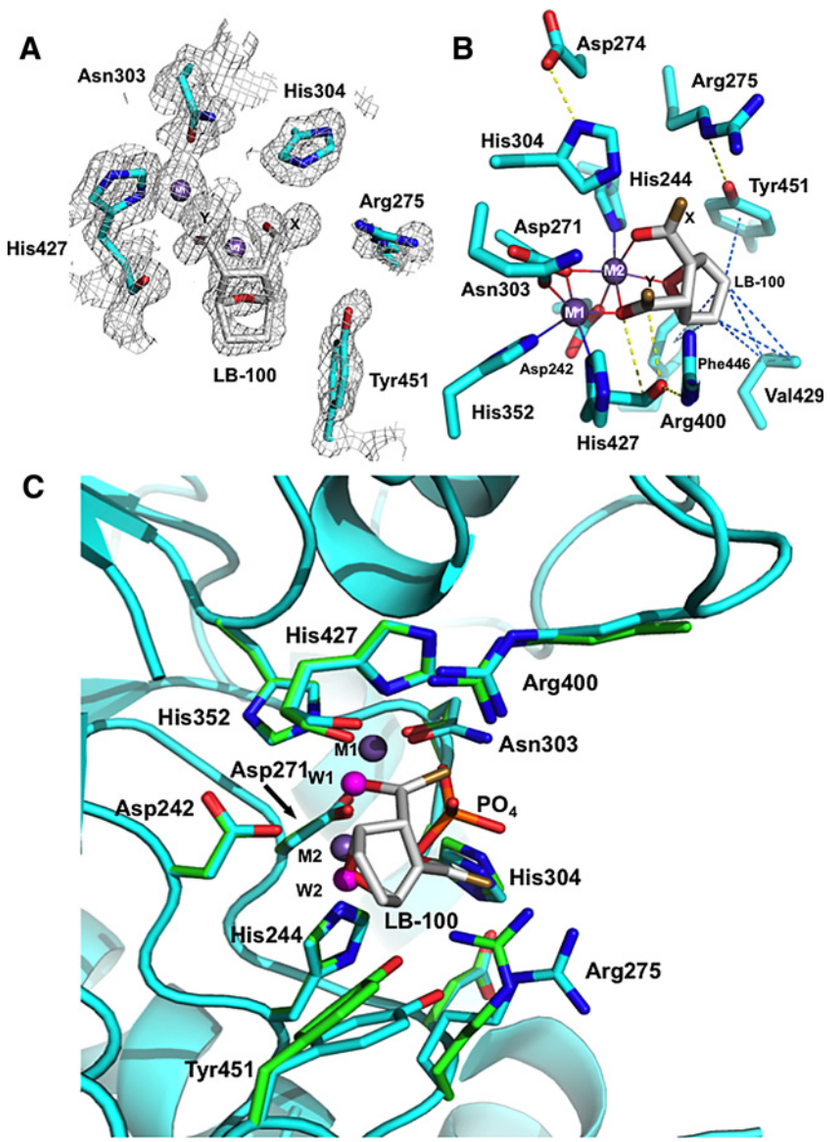

Figure 4.
Representative contacts of the 7-oxabicyclo[2.2.1]heptane-2,3-carbonyl moiety of LB-100 within the active site of PP5C. **A,** Composite omit map generated by Autobuild (PHENIX) contoured at 1σ showing electron density for LB-100, active-site metal ions, and active-site residues. **B,** Stick representation showing the coordination sphere of each metal ion in the LB-100 complex. Carbonyl dipole–dipole stacking interactions and hydrogen bonds are shown as yellow dotted lines, and metal–ligand bonds are shown as solid lines. Hydrophobic contacts between the inhibitor and the side chains of Val429, Phe446, and Tyr451 are represented as blue dotted lines. **C,** Comparison showing superposition of amino acid residues near the active site in the substrate analog complex (PDB code 1S95; ref. 29; green) and the LB-100 complex (cyan). The metal-coordinated waters in the phosphate complex are shown as magenta spheres (W1 and W2). Metal ions (M1 and M2) are shown as purple spheres, and the ambiguous positions X and Y are colored bronze.

as a novel antitumor agent, either alone or in combination with existing therapies (21).

In nearly all reports describing LB-100 activity, the target of LB-100 is ascribed to the specific inhibition of ser/thr protein phosphatase type 2A (PP2A; refs. 21, 23, 25, 27, 80, 81). However, the most cited reference to support selectivity for PP2A (22) was corrected in 2009, revealing that the compound with >10,000-fold selectivity for PP2A was another endothall derivative [LB-102; 4-(3-carboxy-7-oxa-bicyclo [2.2.1] heptane-2-carbonyl)piperazine-1-carboxylic acid tert- butyl ester; Fig. 1]. After a thorough search of the published literature, we could find no experimental evidence documenting the selective engagement of LB-100 with PP2A *in vitro*, in cells or in animals, nor are there reports that tested the ability of LB-100 to inhibit PPP5C activity. The studies described here tested the inhibitory activity of LB-100 against both PP2AC and PPP5C using three different substrates, and, therefore, represent the most comprehensive assessment of the inhibitory activity of LB-100 against PP2A published to date. Our data confirm that LB-100 does indeed act as a catalytic inhibitor of PP2AC. In addition, LB-100 also inhibits the catalytic activity of PPP5C, demonstrating only modest selectivity toward PP2AC (Fig. 2; Table 1). Because LB-100 only demonstrates modest selectivity for PP2AC versus PPP5C and there is no experimental evidence in the published literature for the selective engagement of LB-100 with PP2A *in vitro*, in cells or in animals, we conclude that the observed effects of LB-100 *in vivo* may not be due to the specific inhibition of PP2AC alone.

Our cocrystal structure also defines the binding site of LB-100 in PPP5C, revealing coordination with the catalytic metals in the active site. The ability of LB-100 to inhibit both PP2AC and PPP5C is similar to the actions of cantharidin and endothall, which both show modest selectivity for PP2AC versus PPP5C. The hydrolyzed diacid forms of both cantharidin and endothall share a 7-oxabicyclo[2.2.1]heptane-2,3-dicarbonyl moiety with LB-100, and the crystal structures of PPP5C in complex with cantharidin,

endothall, and two novel cantharidin derivatives have been reported (9). For all five compounds, contacts between the shared core scaffold, catalytic site residues, and metal ions are conserved across these complexes. In our PPP5C-LB-100 structure, there was insufficient density to assign a position for the methylpiperazine ring. This prompted us to re-evaluate the reported stability of LB-100 in order to assess the possibility that the ring was hydrolyzed during storage. MS analysis of the same batch of LB-100, stored for >6 months as a powder and dissolved 3 months prior to generating the stock solution used to make the cocrystals, retained the correct molecular weight even after lyophilization and resuspension (Supplementary Fig. S2). These observations are consistent with previous reports indicating that LB-100 is stable during prolonged storage (21). Therefore, we concluded that the ring does not likely contribute to the retention of LB-100 at the active site of PPP5C.

To date, there are no reports of compounds that act as specific inhibitors of PPP5C. However, in numerous studies of PPP5C function, multiple lines of evidence have revealed a positive correlation between PPP5C overexpression and human cancers, including invasive ductal carcinoma of the breast (38), hepatocarcinogenesis (40), lymphoma (82), glioma (83, 84), colorectal (85), and prostate cancers (86). In cell culture models, PPP5C overexpression aids cancer-cell proliferation and survival during hypoxia (38, 87, 88), and in mouse xenograft models of tumor development, constitutive PPP5C overexpression markedly aids tumor growth (38, 89). Similar to observations made with LB-100 in cell culture, studies conducted with siRNA or antisense oligonucleotides targeting PPP5C-mRNA indicate that the suppression of PPP5C prolongs stress-induced signaling cascades that favor apoptosis and sensitize cancer cells to stress- or drug-induced apoptosis (38, 87, 90–92). Indeed, many actions reported in response to treatment with LB-100 (e.g., Chk1-phosphorylation, AKT-1 phosphorylation, increased sensitivity to doxorubicin) are mimicked by the action of siRNA or antisense oligonucleotides specifically targeting PPP5C (5, 6, 28, 38, 46, 82–84, 86–89, 93). In addition, the suppression of PPP5C is known to augment many actions elicited by GR activation (88, 91, 94), and dexamethasone increased the sensitivity of U-937 cells to LB-100–mediated cytotoxicity (Fig. 3B). We also observed a concentration-dependent increase in the phosphorylation of ribosomal protein S6 after treatment with LB-100, which is also observed when the expression of PPP5C is disrupted using CRISPR-Cas9–based methods (Fig. 3C and D). Together, these studies suggest that many of the actions of LB-100 that were assumed to be due to the specific inhibition of PP2A could result from the inhibition of PP2A, PPP5C, or both PP2A and PPP5C.

Nonetheless, there are also actions of LB-100 that can be mimicked by the specific suppression of PP2A expression. For example, the ability of LB-100 to induce G_2–M arrest or the appearance of aberrant mitotic spindles (21, 22, 24, 25) is mimicked by antisense oligonucleotides targeting PP2AC (7) but is not observed in cells treated with siRNA/antisense oligonucleotides targeting PPP5C (38, 90, 91). Further, the genetic disruption of PPP5C in mice only produces a mild metabolic phenotypic change (93), and HEK-293 cells that do not express PPP5C protein are also viable. In addition, in the absence of genomic stress, the suppression of PPP5C expression with siRNA or antisense oligonucleotides does not induce apoptosis in many types of cells grown in culture (38, 87, 89). These observations argue that the specific inhibition of PPP5 in the absence of hypoxia or treatment with drugs that induced genomic stress/damage may not kill cancer cells unless PP2A is also inhibited. Therefore, future studies should explore the possibility that the observed antitumor activity of LB-100 might be due to an additive affect achieved by suppressing both PP2A and PPP5C.

Finally, it is important to remember that, unlike PPP5C, which encompasses catalytic, targeting, and regulatory function within a single polypeptide chain encoded by a single gene, PP2AC is a catalytic subunit that is shared by many PP2A holoenzyme complexes. A vast array of functional heterotrimeric PP2A-holoenzymes can be assembled combinatorially from a set of two isoforms of the 65 kDa scaffolding subunit, two isoforms of the 36 kDa catalytic subunit, and 18 different regulatory subunits that confer substrate specificity, affect subcellular localization, and/or alter catalytic activity. Therefore, further studies are also needed to determine if the strength of LB-100 binding is altered when PP2AC is assembled into particular holoenzyme complexes or when PPP5C is in complex with known binding partners (95). Future investigations are also needed to assess the ability of LB-100 to inhibit the activity of other PPP-family members that share the same catalytic mechanism, notably PPP6C which is highly sensitive to cantharidin- and other endothall-derived derivatives (9).

Disclosure of Potential Conflicts of Interest

No potential conflicts of interest were disclosed.

Authors' Contributions

Conception and design: B.M. D'Arcy, M.R. Swingle, A. Prakash, R.E. Honkanen
Development of methodology: B.M. D'Arcy, M.R. Swingle, A. Prakash, R.E. Honkanen
Acquisition of data (provided animals, acquired and managed patients, provided facilities, etc.): B.M. D'Arcy, M.R. Swingle, C.M. Papke, K.A. Abney, E.S. Bouska
Analysis and interpretation of data (e.g., statistical analysis, biostatistics, computational analysis): B.M. D'Arcy, M.R. Swingle, C.M. Papke, A. Prakash, R.E. Honkanen
Writing, review, and/or revision of the manuscript: B.M. D'Arcy, M.R. Swingle, A. Prakash, R.E. Honkanen
Administrative, technical, or material support (i.e., reporting or organizing data, constructing databases): K.A. Abney, E.S. Bouska, A. Prakash
Study supervision: A. Prakash, R.E. Honkanen

Acknowledgments

The authors would like to thank Drs. Brian Eckenroth (University of Vermont) and Matthew Benning (Bruker) for technical advice during crystal data collection and structure determination.

This work was supported in part by grants from the NIH (R01CA-60750, R21NS071553, R03MH085702 to R.E. Honkanen; NIEHS grant 5R00ES024417 to A. Prakash). A training grant (NIH T32HL076125) provided a stipend for E.S. Bouska. Funds were also provided by the University of South Alabama Cancer Center Research Fund to A. Prakash, B.M. D'Arcy, and R.E. Honkanen, and the Mayer Mitchell Award for Excellence in Cancer Research (to R.E. Honkanen). This investigation was conducted, in part, in a facility constructed with support from Research Facilities Improvement Program Grant (C06 RR11174) from the National Center for Research Resources.

The costs of publication of this article were defrayed in part by the payment of page charges. This article must therefore be hereby marked *advertisement* in accordance with 18 U.S.C. Section 1734 solely to indicate this fact.

Received November 16, 2017; revised March 20, 2018; accepted January 11, 2019; published first January 24, 2019.

References

1. Wu P, Nielsen TE, Clausen MH. FDA-approved small-molecule kinase inhibitors. Trends Pharmacol Sci 2015;36:422–39.
2. Santos R, Ursu O, Gaulton A, Bento AP, Donadi RS, Bologa CG, et al. A comprehensive map of molecular drug targets. Nat Rev Drug Discov 2017; 16:19–34.
3. Moorhead GB, Trinkle-Mulcahy L, Ulke-Lemee A. Emerging roles of nuclear protein phosphatases. Nat Rev Mol Cell Biol 2007;8:234–44.
4. Liu J, Farmer JD Jr, Lane WS, Friedman J, Weissman I, Schreiber SL. Calcineurin is a common target of cyclophilin-cyclosporin A and FKBP-FK506 complexes. Cell 1991;66:807–15.
5. Honkanen RE, Golden T. Regulators of serine/threonine protein phosphatases at the dawn of a clinical era? Curr Med Chem 2002;9:2055–75.
6. Swingle MR, Amable L, Lawhorn BG, Buck SB, Burke CP, Ratti P, et al. Structure-activity relationship studies of fostriecin, cytostatin, and key analogs, with PP1, PP2A, PP5, and(beta12-beta13)-chimeras (PP1/PP2A and PP5/PP2A), provide further insight into the inhibitory actions of fostriecin family inhibitors. J Pharmacol Exp Ther 2009;331:45–53.
7. Bonness K, Aragon IV, Rutland B, Ofori-Acquah S, Dean NM, Honkanen RE. Cantharidin-induced mitotic arrest is associated with the formation of aberrant mitotic spindles and lagging chromosomes resulting, in part, from the suppression of PP2Aalpha. Mol Cancer Ther 2006;5:2727–36.
8. Honkanen RE. Cantharidin, another natural toxin that inhibits the activity of serine/threonine protein phosphatases types 1 and 2A. FEBS Lett 1993; 330:283–6.
9. Chattopadhyay D, Swingle MR, Salter EA, Wood E, D'Arcy B, Zivanov C, et al. Crystal structures and mutagenesis of PPP-family ser/thr protein phosphatases elucidate the selectivity of cantharidin and novel norcantharidin-based inhibitors of PP5C. Biochem Pharmacol 2016;109:14–26.
10. Lawhorn BG, Boga SB, Wolkenberg SE, Colby DA, Gauss CM, Swingle MR, et al. Total synthesis and evaluation of cytostatin, its C10-C11 diastereomers, and additional key analogues: impact on PP2A inhibition. J Am Chem Soc 2006;128:16720–32.
11. Boger DL, Ichikawa S, Zhong W. Total synthesis of fostriecin (CI-920). J Am Chem Soc 2001;123:4161–7.
12. Swingle MR, Amable L, Lawhorn BG, Buck SB, Burke CP, Ratti P, et al. Structure-activity relationship studies of fostriecin, cytostatin, and key analogs, with PP1, PP2A, PP5, and (β12–β13)-chimeras (PP1/PP2A and PP5/PP2A), provide further insight into the inhibitory actions of fostriecin family inhibitors. J Pharmacol Exp Ther 2009;331:45–53.
13. Lewy DS, Gauss CM, Soenen DR, Boger DL. Fostriecin: chemistry and biology. Curr Med Chem 2002;9:2005–32.
14. Buck SB, Hardouin C, Ichikawa S, Soenen DR, Gauss CM, Hwang I, et al. Fundamental role of the fostriecin unsaturated lactone and implications for selective protein phosphatase inhibition. J Am Chem Soc 2003;125: 15694–5.
15. Le LH, Erlichman C, Pillon L, Thiessen JJ, Day A, Wainman N, et al. Phase I and pharmacokinetic study of fostriecin given as an intravenous bolus daily for five consecutive days. Invest New Drugs 2004;22:159–67.
16. Wang GS. Medical uses of mylabris in ancient China and recent studies. J Ethnopharmacol 1989;26:147–62.
17. Li YM, Casida JE. Cantharidin-binding protein: identification as protein phosphatase 2A. Proc Natl Acad Sci U S A 1992;89:11867–70.
18. Honkanen RE, Zwiller J, Moore RE, Daily SL, Khatra BS, Dukelow M, et al. Characterization of microcystin-LR, a potent inhibitor of type 1 and type 2A protein phosphatases. J Biol Chem 1990;265:19401–4.
19. Honkanen RE, Dukelow M, Zwiller J, Moore RE, Khatra BS, Boynton AL. Cyanobacterial nodularin is a potent inhibitor of type 1 and type 2A protein phosphatases. Mol Pharmacol 1991;40:577–83.
20. Hill TA, Stewart SG, Sauer B, Gilbert J, Ackland SP, Sakoff JA, et al. Heterocyclic substituted cantharidin and norcantharidin analogues—synthesis, protein phosphatase (1 and 2A) inhibition, and anti-cancer activity. Bioorg Med Chem Lett 2007;17:3392–7.
21. Chung V, Mansfield AS, Braiteh F, Richards D, Durivage H, Ungerleider RS, et al. Safety, tolerability, and preliminary activity of LB-100, an inhibitor of protein phosphatase 2A, in patients with relapsed solid tumors: an open-label, dose escalation, first-in-human, phase I trial. Clin Cancer Res 2017; 23:3277–84.
22. Lu J, Kovach JS, Johnson F, Chiang J, Hodes R, Lonser R, et al. Inhibition of serine/threonine phosphatase PP2A enhances cancer chemotherapy by blocking DNA damage induced defense mechanisms. Proc Natl Acad Sci U S A 2009;106:11697–702.
23. Bai X, Zhi X, Zhang Q, Liang F, Chen W, Liang C, et al. Inhibition of protein phosphatase 2A sensitizes pancreatic cancer to chemotherapy by increasing drug perfusion via HIF-1alpha-VEGF mediated angiogenesis. Cancer Lett 2014;355:281–7.
24. Lv P, Wang Y, Ma J, Wang Z, Li JL, Hong CS, et al. Inhibition of protein phosphatase 2A with a small molecule LB100 radiosensitizes nasopharyngeal carcinoma xenografts by inducing mitotic catastrophe and blocking DNA damage repair. Oncotarget 2014;5:7512–24.
25. Bai XL, Zhang Q, Ye LY, Hu QD, Fu QH, Zhi X, et al. Inhibition of protein phosphatase 2A enhances cytotoxicity and accessibility of chemotherapeutic drugs to hepatocellular carcinomas. Mol Cancer Ther 2014;13: 2062–72.
26. Zhang C, Peng Y, Wang F, Tan X, Liu N, Fan S, et al. A synthetic cantharidin analog for the enhancement of doxorubicin suppression of stem cell-derived aggressive sarcoma. Biomaterials 2010;31:9535–43.
27. Fu QH, Zhang Q, Zhang JY, Sun X, Lou Y, Li GG, et al. LB-100 sensitizes hepatocellular carcinoma cells to the effects of sorafenib during hypoxia by activation of Smad3 phosphorylation. Tumour Biol 2016;37: 7277–86.
28. Swingle MR, Honkanen RE, Ciszak EM. Structural basis for the catalytic activity of human serine/threonine protein phosphatase-5. J Biol Chem 2004;279:33992–9.
29. Sablina AA, Hector M, Colpaert N, Hahn WC. Identification of PP2A complexes and pathways involved in cell transformation. Cancer Res 2010;70:10474–84.
30. Dushukyan N, Dunn DM, Sager RA, Woodford MR, Loiselle DR, Daneshvar M, et al. Phosphorylation and ubiquitination regulate protein phosphatase 5 activity and its prosurvival role in kidney cancer. Cell Rep 2017;21: 1883–95.
31. Yong WH, Ueki K, Chou D, Reeves SA, VONDEIMLING A, Gusella JF, et al. Cloning of a highly conserved human protein serine-threonine phosphatase gene from the glioma candidate region on chromosome 19q13. 3. Genomics 1995;29:533–6.
32. Han K, Gan Z, Lin S, Hu H, Shen Z, Min D. Elevated expression of serine/threonine phosphatase type 5 correlates with malignant proliferation in human osteosarcoma. Acta Biochim Pol 2017;64:11–6.
33. Zhi X, Zhang H, He C, Wei Y, Bian L, Li G. Serine/threonine protein phosphatase-5 accelerates cell growth and migration in human glioma. Cell Mol Neurobiol 2015;35:669–77.
34. Golden T, Aragon IV, Zhou G, Cooper SR, Dean NM, Honkanen RE. Constitutive over expression of serine/threonine protein phosphatase 5 (PP5) augments estrogen-dependent tumor growth in mice. Cancer Lett 2004;215:95–100.
35. Ghobrial IM, McCormick DJ, Kaufmann SH, Leontovich AA, Loegering DA, Dai NT, et al. Proteomic analysis of mantle-cell lymphoma by protein microarray. Blood 2005;105:3722–30.
36. Urban G, Golden T, Aragon IV, Scammell JG, Dean NM, Honkanen RE. Identification of an estrogen-inducible phosphatase (PP5) that converts MCF-7 human breast carcinoma cells into an estrogen-independent phenotype when expressed constitutively. J Biol Chem 2001;276: 27638–46.
37. von Kriegsheim A, Pitt A, Grindlay GJ, Kolch W, Dhillon AS. Regulation of the Raf–MEK–ERK pathway by protein phosphatase 5. Nat Cell biol 2006; 8:1011–6.
38. Golden T, Aragon IV, Rutland B, Tucker JA, Shevde LA, Samant RS, et al. Elevated levels of Ser/Thr protein phosphatase 5 (PP5) in human breast cancer. Biochim Biophys Acta 2008;1782:259–70.
39. Zheng X, Zhang L, Jin B, Zhang F, Zhang D, Cui L. Knockdown of protein phosphatase 5 inhibits ovarian cancer growth in vitro. Oncol Lett 2016;11: 168–72.
40. Chen YL, Hung MH, Chu PY, Chao TI, Tsai MH, Chen LJ, et al. Protein phosphatase 5 promotes hepatocarcinogenesis through interaction with AMP-activated protein kinase. Biochem Pharmacol 2017;138:49–60.
41. Gu Y, Barzegar M, Chen X, Wu Y, Shang C, Mahdavian E, et al. Fusarochromanone-induced reactive oxygen species results in activation of JNK cascade and cell death by inhibiting protein phosphatases 2A and 5. Oncotarget 2015;6:42322–33.

42. Wang J, Zhu J, Dong M, Yu H, Dai X, Li K. Inhibition of protein phosphatase 5 (PP5) suppresses survival and growth of colorectal cancer cells. Biotechnol Appl Biochem 2015;62:621–7.
43. Vaughan CK, Mollapour M, Smith JR, Truman A, Hu B, Good VM, et al. Hsp90-dependent activation of protein kinases is regulated by chaperone-targeted dephosphorylation of Cdc37. Mol Cell 2008;31:886–95.
44. Swingle M, Volmar CH, Saldanha SA, Chase P, Eberhart C, Salter EA, et al. An ultra-high-throughput screen for catalytic inhibitors of serine/threonine protein phosphatases types 1 and 5 (PP1C and PP5C). SLAS Discov 2017;22:21–31.
45. Sittampalam GS, Coussens NP, Brimacombe K, Grossman A, Arkin M, Auld D, et al. Assay guidance manual. Bethesda, MD: Eli Lily & Company and the National Center for Advancing Translational Sciences; 2004.
46. Ni L, Swingle MS, Bourgeois AC, Honkanen RE. High yield expression of serine/threonine protein phosphatase type 5, and a fluorescent assay suitable for use in the detection of catalytic inhibitors. Assay Drug Dev Technol 2007;5:645–53.
47. Swingle M, Ni L, Honkanen RE. Small-molecule inhibitors of ser/thr protein phosphatases: specificity, use and common forms of abuse. Methods Mol Biol 2007;365:23–38.
48. Adams PD, Afonine PV, Bunkoczi G, Chen VB, Davis IW, Echols N, et al. PHENIX: a comprehensive Python-based system for macromolecular structure solution. Acta Crystallogr D Biol Crystallogr 2010;66:213–21.
49. Afonine PV, Grosse-Kunstleve RW, Echols N, Headd JJ, Moriarty NW, Mustyakimov M, et al. Towards automated crystallographic structure refinement with phenix.refine. Acta Crystallogr D Biol Crystallogr 2012;68:352–67.
50. Emsley P, Lohkamp B, Scott WG, Cowtan K. Features and development of Coot. Acta Crystallogr Sect D 2010;66:486–501.
51. Emsley P, Cowtan K. Coot: model-building tools for molecular graphics. Acta Crystallogr Sect D 2004;60:2126–32.
52. Chen VB, Arendall WB 3rd, Headd JJ, Keedy DA, Immormino RM, Kapral GJ, et al. MolProbity: all-atom structure validation for macromolecular crystallography. Acta Crystallogr D Biol Crystallogr 2010;66:12–21.
53. Amable L, Grankvist N, Largen JW, Ortsater H, Sjoholm A, Honkanen RE. Disruption of serine/threonine protein phosphatase 5 (PP5:PPP5c) in mice reveals a novel role for PP5 in the regulation of ultraviolet light-induced phosphorylation of serine/threonine protein kinase Chk1 (CHEK1). J Biol Chem 2011;286:40413–22.
54. Mazalouskas MD, Godoy-Ruiz R, Weber DJ, Zimmer DB, Honkanen RE, Wadzinski BE. Small G proteins Rac1 and Ras regulate serine/threonine protein phosphatase 5 (PP5).extracellular signal-regulated kinase (ERK) complexes involved in the feedback regulation of Raf1. J Biol Chem 2014;289:4219–32.
55. Lee HJ, Hwang HI, Jang YJ. Mitotic DNA damage response: Polo-like kinase-1 is dephosphorylated through ATM-Chk1 pathway. Cell Cycle 2010;9:2389–98.
56. Wei D, Parsels LA, Karnak D, Davis MA, Parsels JD, Marsh AC, et al. Inhibition of protein phosphatase 2A radiosensitizes pancreatic cancers by modulating CDC25C/CDK1 and homologous recombination repair. Clin Cancer Res 2013;19:4422–32.
57. Hu C, Yu M, Ren Y, Li K, Maggio DM, Mei C, et al. PP2A inhibition from LB100 therapy enhances daunorubicin cytotoxicity in secondary acute myeloid leukemia via miR-181b-1 upregulation. Sci Rep 2017;7:2894.
58. Zhang C, Hong CS, Hu X, Yang C, Wang H, Zhu D, et al. Inhibition of protein phosphatase 2A with the small molecule LB100 overcomes cell cycle arrest in osteosarcoma after cisplatin treatment. Cell Cycle 2015;14:2100–8.
59. Dai C, Zhang X, Xie D, Tang P, Li C, Zuo Y, et al. Targeting PP2A activates AMPK signaling to inhibit colorectal cancer cells. Oncotarget 2017;8:95810.
60. Ho WS, Feldman MJ, Maric D, Amable L, Hall MD, Feldman GM, et al. PP2A inhibition with LB100 enhances cisplatin cytotoxicity and overcomes cisplatin resistance in medulloblastoma cells. Oncotarget 2016;7:12447.
61. Lv P, Wang Y, Ma J, Wang Z, Li JL, Hong CS, et al. Inhibition of protein phosphatase 2A with a small molecule LB100 radiosensitizes nasopharyngeal carcinoma xenografts by inducing mitotic catastrophe and blocking DNA damage repair. Oncotarget 2014;5:7512.
62. Bai XL, Zhang Q, Ye LY, Hu QD, Fu QH, Zhi X, et al. Inhibition of protein phosphatase 2A enhances cytotoxicity and accessibility of chemotherapeutic drugs to hepatocellular carcinomas. Mol Cancer Thera 2014;13:2062–72.
63. Gordon IK, Lu J, Graves CA, Huntoon K, Frerich JM, Hanson RH, et al. Protein phosphatase 2A inhibition with LB100 enhances radiation-induced mitotic catastrophe and tumor growth delay in glioblastoma. Mol Cancer Thera 2015;14:1540–7.
64. Chang KE, Wei BR, Madigan JP, Hall MD, Simpson RM, Zhuang Z, et al. The protein phosphatase 2A inhibitor LB100 sensitizes ovarian carcinoma cells to cisplatin-mediated cytotoxicity. Mol Cancer Thera 2014;14:90–100.
65. Bonness K, Aragon IV, Rutland B, Ofori-Acquah S, Dean NM, Honkanen RE. Cantharidin-induced mitotic arrest is associated with the formation of aberrant mitotic spindles and lagging chromosomes resulting, in part, from the suppression of PP2Aα. Mol Cancer Thera 2006;5:2727–36.
66. Ramsey AJ, Chinkers M. Identification of potential physiological activators of protein phosphatase 5. Biochemistry 2002;41:5625–32.
67. Kang H, Sayner SL, Gross KL, Russell LC, Chinkers M. Identification of amino acids in the tetratricopeptide repeat and C-terminal domains of protein phosphatase 5 involved in autoinhibition and lipid activation. Biochemistry 2001;40:10485–90.
68. Morita K, Saitoh M, Tobiume K, Matsuura H, Enomoto S, Nishitoh H, et al. Negative feedback regulation of ASK1 by protein phosphatase 5 (PP5) in response to oxidative stress. EMBO J 2001;20:6028–36.
69. Huang S, Shu L, Easton J, Harwood FC, Germain GS, Ichijo H, et al. Inhibition of mammalian target of rapamycin activates apoptosis signal-regulating kinase 1 signaling by suppressing protein phosphatase 5 activity. J Biol Chem 2004;279:36490–6.
70. Sekine Y, Hatanaka R, Watanabe T, Sono N, Iemura S, Natsume T, et al. The Kelch repeat protein KLHDC10 regulates oxidative stress-induced ASK1 activation by suppressing PP5. Mol Cell 2012;48:692–704.
71. Zhou G, Golden T, Aragon IV, Honkanen RE. Ser/Thr protein phosphatase 5 inactivates hypoxia-induced activation of an apoptosis signal-regulating kinase 1/MKK-4/JNK signaling cascade. J Biol Chem 2004;279:46595–605.
72. Chen MS, Silverstein AM, Pratt WB, Chinkers M. The tetratricopeptide repeat domain of protein phosphatase 5 mediates binding to glucocorticoid receptor heterocomplexes and acts as a dominant negative mutant. J Biol Chem 1996;271:32315–20.
73. Zuo Z, Urban G, Scammell JG, Dean NM, McLean TK, Aragon I, et al. Ser/Thr protein phosphatase type 5 (PP5) is a negative regulator of glucocorticoid receptor-mediated growth arrest. Biochemistry 1999;38:8849–57.
74. Bouazza B, Krytska K, Debba-Pavard M, Amrani Y, Honkanen RE, Tran J, et al. Cytokines alter glucocorticoid receptor phosphorylation in airway cells: role of phosphatases. Am J Respir Cell Mol Biol 2012;47:464–73.
75. Tommasini I, Cantoni O. Dexamethasone promotes toxicity in U937 cells exposed to otherwise nontoxic concentrations of peroxynitrite: pivotal role for lipocortin 1-mediated inhibition of cytosolic phospholipase A2. Mol Pharmacol 2004;65:964–72.
76. Tommasini I, Sestili P, Guidarelli A, Cantoni O. Hydrogen peroxide generated at the level of mitochondria in response to peroxynitrite promotes U937 cell death via inhibition of the cytoprotective signalling mediated by cytosolic phospholipase A 2. Cell Death Differ 2004;11:974.
77. Tommasini I, Sestili P, Guidarelli A, Cantoni O. Peroxynitrite stimulates the activity of cytosolic phospholipase A 2 in U937 cells: the extent of arachidonic acid formation regulates the balance between cell survival or death. Cell Death Differ 2002;9:1368.
78. Swingle M, Ni L, Honkanen RE. Small-molecule inhibitors of Ser/Thr protein phosphatases. Protein phosphatase protocols. Totowa, NJ: Springer; 2007. p. 23–38.
79. Hamilton CL, Abney KA, Vasauskas AA, Alexeyev M, Ni L, Honkanen RE, et al. Serine/threonine phosphatase 5 (PP5C/PPP5C) regulates the ISOC channel through a PP5C-FKBP51 axis. Pulm Circ 2018;8:2045893217753156.
80. Hong CS, Ho W, Zhang C, Yang C, Elder JB, Zhuang Z. LB100, a small molecule inhibitor of PP2A with potent chemo- and radio-sensitizing potential. Cancer Biol Ther 2015;16:821–33.
81. Fu X, Sun F, Wang F, Zhang J, Zheng B, Zhong J, et al. Aloperine protects mice against DSS-induced colitis by PP2A-mediated PI3K/Akt/mTOR signaling suppression. Mediators Inflamm 2017;2017:5706152.
82. Ghobrial IM, McCormick DJ, Kaufmann SH, Leontovich AA, Loegering DA, Dai NT, et al. Proteomic analysis of mantle-cell lymphoma by protein microarray. Blood 2005;105:3722–30.

83. Zhi X, Zhang H, He C, Wei Y, Bian L, Li G. Serine/threonine protein phosphatase-5 accelerates cell growth and migration in human glioma. Cell Mol Neurobiol 2015;35:669–77.
84. Yong WH, Ueki K, Chou D, Reeves SA, von Deimling A, Gusella JF, et al. Cloning of a highly conserved human protein serine-threonine phosphatase gene from the glioma candidate region on chromosome 19q13.3. Genomics 1995;29:533–6.
85. Wang J, Zhu J, Dong M, Yu H, Dai X, Li K. Inhibition of protein phosphatase 5 (PP5) suppresses survival and growth of colorectal cancer cells. Biotechnol Appl Biochem 2014;62:621–7.
86. Taira J, Higashimoto Y. Caveolin-1 interacts with protein phosphatase 5 and modulates its activity in prostate cancer cells. Biochem Biophys Res Commun 2013;431:724–8.
87. Zhou G, Golden T, Aragon IV, Honkanen RE. Ser/Thr protein phosphatase 5 inactivates hypoxia-induced activation of an apoptosis signal-regulating kinase 1/MKK-4/JNK signaling cascade. J Biol Chem 2004;279: 46595–605.
88. Golden T, Swingle M, Honkanen RE. The role of serine/threonine protein phosphatase type 5 (PP5) in the regulation of stress-induced signaling networks and cancer. Cancer Metastasis Rev 2008;27:169–78.
89. Golden T, Aragon IV, Zhou G, Cooper SR, Dean NM, Honkanen RE. Constitutive over expression of serine/threonine protein phosphatase 5 (PP5) augments estrogen-dependent tumor growth in mice. Cancer Lett 2004;215:95–100.
90. Zuo Z, Dean NM, Honkanen RE. Serine/threonine protein phosphatase type 5 acts upstream of p53 to regulate the induction of p21(WAF1/Cip1) and mediate growth arrest. J Biol Chem 1998;273:12250–8.
91. Zuo Z, Urban G, Scammell JG, Dean NM, McLean TK, Aragon I, et al. Ser/Thr protein phosphatase type 5 (PP5) is a negative regulator of glucocorticoid receptor-mediated growth arrest. Biochemistry 1999;38:8849–57.
92. von Kriegsheim A, Pitt A, Grindlay GJ, Kolch W, Dhillon AS. Regulation of the Raf-MEK-ERK pathway by protein phosphatase 5. Nat Cell Biol 2006;8: 1011–6.
93. Grankvist N, Honkanen RE, Sjoholm A, Ortsater H. Genetic disruption of protein phosphatase 5 in mice prevents high-fat diet feeding-induced weight gain. FEBS Lett 2013;587:3869–74.
94. Fransson L, Rosengren V, Saha TK, Grankvist N, Islam T, Honkanen RE, et al. Mitogen-activated protein kinases and protein phosphatase 5 mediate glucocorticoid-induced cytotoxicity in pancreatic islets and beta-cells. Mol Cell Endocrinol 2014;383:126–36.
95. Skarra DV, Goudreault M, Choi H, Mullin M, Nesvizhskii AI, Gingras AC, et al. Label-free quantitative proteomics and SAINT analysis enable interactome mapping for the human Ser/Thr protein phosphatase 5. Proteomics 2011;11:1508–16.